

Investigation of the biological and anti-cancer properties of ellagic acid-encapsulated nano-sized metalla-cages

Abhishek Dubey^{1,*}
 Dae Won Park^{2,*}
 Jung Eun Kwon²
 Yong Joon Jeong²
 Taegeun Kim¹
 Inhye Kim³
 Se Chan Kang²
 Ki-Whan Chi¹

¹Department of Chemistry, University of Ulsan, Ulsan, ²Department of Life Science, Gachon University, Seongnam, ³Laboratory of Bio-Resources, Yongin-si, Gyeonggi-Do, Republic of Korea

*These authors contributed equally to this work

Correspondence: Ki-Whan Chi
 Department of Chemistry, University of Ulsan, Ulsan 680-749, Republic of Korea
 Tel +82 52 259 2344
 Fax +82 52 259 2344
 Email kwchi@ulsan.ac.kr

Se Chan Kang
 Department of Life Science, Gachon University, Seongnam 461-701, Republic of Korea
 Tel +82 31 750 8826
 Fax +82 31 750 8984
 Email sckang73@gachon.ac.kr

Abstract: Three new large hexanuclear metalla-prisms **9–11** incorporating 1,3,5-tris(pyridin-4-ylethynyl)benzene (tpeb) **4** and one of the dinuclear arene ruthenium clips [Ru₂(*p*-iPrC₆H₄Me)₂(OO \cap OO)] [CF₃SO₃]₂ (OO \cap OO = 2,5-dioxydo-1,4-benzoquinonato [dobq] **1**, 5,8-dihydroxy-1,4-naphthaquinonato (donq) **2**, and 6,11-dihydroxy-5,12-naphthacenedionato [dotq] **3**), which encapsulate the guest molecule ellagic acid (2,3,7,8-tetrahydroxychromeno[5,4,3-cde]chromene-5,10-dione, **5**) were prepared. All complexes were isolated as triflate salts in good yields and were fully characterized by ¹H NMR spectroscopy and electrospray ionization mass spectrometry. The photophysical properties of these metalla-prisms were also investigated. Compounds **9** and **10** showed potent antioxidant activity, but **10** had the superior ORAC_{PE} value (1.30±0.020). Ellagic acid (**5**) and compound **11** showed weaker activity than that of Trolox. The 3-(4,5-dimethylthiazol-2-yl)-2,5-diphenyltetrazolium bromide assay showed that the metalla-prism compounds exhibit anticancer properties in vitro. Compound **10** inhibited the growth of all cancer cell lines at micromolar concentrations, with the highest cytotoxicity observed against A549 human lung cancer cells (IC₅₀ = 25.9 μM). However, these compounds had a lower anti-cancer activity than that of doxorubicin. In a tumoricidal assay, ellagic acid (**5**) and compound **10** induced cytotoxicity in tumor cells, while doxorubicin did not. While free ellagic acid had no effect on the granulocyte-colony stimulating factor and regulated on activation normal T cell expressed and secreted protein, the encapsulated metalla-prism **10** stimulated granulocyte-colony stimulating factor and reduced regulated on activation normal T cell expressed and secreted protein expression in the RAW264.7 macrophage line. Our results show that ellagic acid encapsulated in metalla-prisms inhibited cancer cells via the modulation of mRNA induction and protein expression levels of the granulocyte-colony stimulating factor and regulated on activation normal T cell expressed and secreted protein in macrophages.

Keywords: metalla-prism, antioxidant, tumoricidal assay, G-CSF, Rantes

Introduction

Since the past decade, there has been an increasing amount of interest in the design and synthesis of discrete 3D metallo-supramolecular architectures, as well as in their potential applications ranging from host–guest chemistry,^{1,2} catalysis,^{3–6} and light harvesting^{7–9} to biology.^{10–19} Three-dimensional cages, engineered via coordination-driven self-assembly paradigms, have distinct advantages over conventional covalent-container molecules, owing to the synthetic ease with which the coordination cages can be assembled, the availability of a large library of building blocks, and the ability to design selective guest encapsulations.^{20,21} The strong and highly directional nature of metal–ligand interactions results in the formation of stable and rigid coordination

cages with well-defined internal cavities while the confined nanospaces in these coordination cages create unique environments and geometric constraints distinct from the bulk media.^{16–19} Furthermore, the physicochemical properties of the host–guest complex are generally superior to those of the guest alone, resulting in improved efficacy and biocompatibility.^{22,23} The most widely used metal-based anti-cancer drug, cisplatin,^{24–26} has been encapsulated in various hosts to reduce the severe side effects associated with this treatment.^{27,28} The field is now entering a new era in which applications such as micro-reactors or transporters are leading to new perspectives for metalla-cages.²⁹

Macrophages represent a type of white blood cell that digests dead cell debris, xenobiotics, foreign substances, and cancer cells in a process called phagocytosis. In some situations, macrophages are tumoricidal, selectively recognizing and destroying tumor cells.³⁰ However, the general role of macrophages in tumorigenesis is widely disputed and data suggest that it may be largely dependent on the context of the specific tumor type.³¹ Ellagic acid (**5**) is a secondary metabolite of many natural plants, particularly fruits such as strawberry, cranberry, and raspberry.³² In nature, ellagic acid exists both in the free form and is complexed in the form of ellagitannins. It is a strong antioxidant, and when a dose above the expected dietary intake was administered, it was found to be effective against various tumors.³³ Animal studies demonstrated that only a limited fraction of the ingested ellagic acid is bioavailable,³⁴ since most of it accumulates in intestinal epithelial cells with limited absorption into the circulation. Once absorbed, ellagic acid has a short half-life in the body owing to rapid metabolism in the liver and excretion in the urine.³⁵ Recently, poly(D,L-lactic-co-glycolic acid)–poly(ethylene glycol) (PLGA–PEG) nanoparticles loaded with ellagic acid were shown to have a chemo-preventive effect in MCF-7 human breast cancer cells.³⁶ Although anticancer and cancer preventive effects of ellagic acid as an antioxidant have been reported, there is no information on the tumoricidal mechanism. In this study, we investigated whether the effect of ellagic acid could be mediated via ligands released by macrophages.

We have previously reported the preparation of various hexanuclear metalla-prisms,^{14,19} which were investigated as candidates for anti-cancer therapy. Following our results, we hypothesized that the encapsulation of ellagic acid (**5**) in hexanuclear metalla-prisms would increase the bioavailability and thereby, also the anticancer activity. We therefore synthesized ellagic acid encapsulated in nano-sized metalla-prisms [ellagic acid \subset Ru₆(*p*-iPrC₆H₄Me)₆(tpeb)₂(dobq)₃][CF₃SO₃]₆ (**9**),

[ellagic acid \subset Ru₆(*p*-iPrC₆H₄Me)₆(tpeb)₂(donq)₃][CF₃SO₃]₆ (**10**) and [ellagic acid \subset Ru₆(*p*-iPrC₆H₄Me)₆(tpeb)₂(dotq)₃][CF₃SO₃]₆ (**11**) (where, tpeb is 1,3,5-tris(pyridin-4-ylethynyl) benzene, dobq is 2,5-dioxydo-1,4-benzoquinonato, donq is 5,8-dihydroxy-1,4-naphthaquinonato and dotq is 6,11-dihydroxy-5,12-naphthacenedionato) with similarly sized cavities but differently sized portals. The antioxidant activities of the compounds were examined by performing an oxygen-radical absorbance capacity (ORAC) assay and the anti-cancer activities by assaying cytokines secreted by macrophages. We found that one of our preparations exhibited tumoricidal effects via the modulation of macrophage-secreted ligands.

Materials and methods

ORAC assay

The ORAC assay was performed essentially as described by Gillespie.³⁷ β -Phycoerythrin (β -PE) and 2,2'-azobis (2-methylpropionamide)dihydrochloride were used as a fluorescent probe and peroxy radical generator, respectively.³⁸ Briefly, 20 μ L of the sample or Trolox was incubated with 10 μ M β -PE and 50 mM 2,2'-azobis (2-methylpropionamide)dihydrochloride in a total volume of 200 μ L. The fluorescence was monitored at 37°C for 60 minutes, at two-minute intervals. All ORAC analyses were performed on a Synergy HT plate reader (Biotek Instruments Inc., Winooski, VT, USA) at 37°C with an excitation wavelength of 530 nm and an emission wavelength of 590 nm. The area under the fluorescence decay curve (AUC) was calculated as follows:

$$\text{AUC} = 1 + \frac{f_1}{f_0} + \frac{f_2}{f_0} + \frac{f_3}{f_0} + \dots + \frac{f_{19}}{f_0} + \frac{f_{20}}{f_0}$$

where f_0 is the initial fluorescence reading at 0 minutes and f_i is the fluorescence reading at i minutes. The net AUC was obtained by subtracting the AUC value of the blank from that of a sample. The protective effect of an antioxidant was measured by comparing the AUC value of the sample with that of a known antioxidant, Trolox, a water-soluble analog of vitamin E. The final results (ORAC values) were calculated and expressed using Trolox equivalents per gram dry weight.

Cancer cell growth inhibition assay

Cell lines such as SK-hep-1 (human hepatocellular carcinoma), AGS (human gastric carcinoma), A549 (human lung carcinoma), and B16/F10 (mouse skin carcinoma) were routinely grown in Dulbecco's Modified Eagle's Medium (DMEM) and Roswell Park Memorial Institute-1640

supplemented with 10% heat inactivated fetal bovine serum, 1% penicillin/streptomycin at 37°C and 5% CO₂. The cell suspensions were seeded in 96-well plates at a concentration of 1×10⁴ cells per well (90 μL per well and 10 μL of the sample). (3-(4,5-Dimethylthiazol-2-yl)-2,5-diphenyltetrazolium bromide) (MTT) was prepared as a stock solution of 5 mg/mL in phosphate buffer saline (pH 7.2) and was filtered. Ten microliters of the MTT solution was added to each well. After incubation for 3 hours at 37°C and 5% CO₂, 100 μL of dimethylsulfoxide was added to each well to lyse the cells. The plates were read by using a multi-reader (Tecan, Männedorf, Switzerland) at 550 nm to determine cell viability, and the percentage of surviving cells was calculated from the ratio of the absorbance of treated to untreated cells. The half-maximal inhibitory concentration (IC₅₀) values for the inhibition of cell growth were determined by comparing the logarithmic plot of the percentage of surviving cells against the concentration of the drug by using a linear regression function.

Macrophage-mediated tumoricidal activity

The mouse macrophage cell line RAW264.7 was cultured in DMEM supplemented with 10% heat-inactivated fetal bovine serum. The assay for macrophage cytotoxicity was based on an assay described previously.³⁹ The cytotoxicity was determined by measuring the viability of tumor target cells after co-cultivation with macrophages for 24 hours. Macrophages (1×10⁵ cells per well) were first incubated for 24 hours in 96-well plates in a medium with or without the test compounds. The macrophages were then washed three times with DMEM–fetal bovine serum and co-cultured for an additional 24 hours with B16/F10 tumor cells at a ratio of 10:1 (1×10⁴ cells per well). At the end of this time, 10 μL of MTT solution (5 mg/mL) was added to each well and incubated for 4 hours at 37°C in an atmosphere of 5% CO₂ before the color was extracted by 100 μL of dimethylsulfoxide added to each well. Cell viability was determined by the absorbance measured at 550 nm read by using a multi-reader (Tecan).

Enzyme-linked immunosorbent assay array

For the determination of secretion of 23 cytokines (tumor necrosis factor-α, insulin-like growth factor, vascular endothelial growth factor, interleukin-6, fibroblast growth factor 6, interferon gamma [IFNγ], epidermal growth factor, leptin, interleukin-1 α, interleukin-1 β, granulocyte-colony stimulating factor [G-CSF], granulocyte-macrophage

colony-stimulating factor, monocyte chemoattractant protein-1, macrophage inflammatory protein-1 α, Skp, cullin, F-box-containing complex, regulated on activation normal T cell expressed and secreted [Rantes], platelet-derived growth factor, beta-nerve growth factor, interleukin-17A, interleukin-2, interleukin-4, interleukin-10, and resistin), RAW264.7 macrophages were incubated for 24 hours with ellagic acid (100 μM) and compound **10** (2 μM), or the medium alone. The levels of the 23 cytokines were determined using a Mouse Cytokine ELISA Plate Array I kit (Signosis, Wyatt Dr Santa Clara, CA, USA) according to the manufacturer's instructions.

Real-time PCR

Total RNA was extracted from RAW264.7 cells using the PureLink™ RNA Mini Kit (Ambion, Foster city, CA, USA). One microgram of total RNA was reversely transcribed in a volume of 20 μL using oligo (dT) primers, with enzyme and buffer supplied in the PrimeScript II 1st strand cDNA synthesis kit (Takara, Osaka, Japan). Quantitative real-time polymerase chain reactions were performed by using a MX3005P qPCR system (Stratagene, La Jolla, CA, USA). The oligonucleotide primers for the murine factors were as follows: for G-CSF, 5'-ATGGCTCAACTTTCTGCCAG-3' (forward) and 5'-CTGACAGTGACCAGGGGAAC-3' (reverse); for Rantes, 5'-ACCCAGCAGTCGTCTTTGTCAC-3' (forward) and 5'-TCCCGAACCCATTTCTTCTCT-3' (reverse), and for β-actin, 5'-GGCTGTATTCCCCTCCATCG-3' (forward) and 5'-CCAGTTGGTAACAATGCCATGT-3' (reverse). The SYBR Premix Ex Taq II kit (Takara) was used for real-time PCR measurements. The final volume of the reaction was 25 μL containing 2 μL of the cDNA template, 12.5 μL of Master Mix, 1 μL of each primer (10 μM stock solution), and 8.5 μL of sterile distilled water. The thermal cycling profile consisted of a pre-incubation step at 95°C for 10 minutes, followed by 40 cycles of 95°C (15 seconds) and 60°C (60 seconds). The relative quantitative evaluation of adipocyte differentiation and lipogenesis at the gene level was performed using the comparative cycle threshold method.

Synthesis of the metalla-prismatic cage **9**

A mixture of tripodal donor **4** (3.0 mg, 0.008 mmol), ruthenium acceptor **1** (10.8 mg, 0.012 mmol), and the guest molecule ellagic acid (1.2 mg, 0.004 mmol) in CH₃OH/CH₃NO₂ (2 mL, 1:1) was stirred at 40°C for 24 hours. The reaction mixture was then filtered and concentrated by using rotavapor to reduce the volume followed by the addition of diethyl ether which yielded **9** as a wine-red crystalline powder. Yield 92%;

^1H NMR (300 MHz, $\text{CD}_3\text{NO}_2:\text{CD}_3\text{OD}$ [1:1] solution, ppm): δ 8.33 (d, $J=4.5$ Hz, 12H), 7.47 (d, $J=4.5$ Hz, 12H), 7.11 (s, 8H), 5.99 (d, $J=5.5$ Hz, 12H), 5.85 (s, 6H), 5.77 (d, $J=5.5$ Hz, 12H), 2.90 (d, $J=6.8$ Hz, 6H), 2.20 (s, 18H), 1.34 (d, $J=6.8$ Hz, 36H); MS (ESI) for **9** ($\text{C}_{152}\text{H}_{126}\text{F}_{18}\text{N}_6\text{O}_{38}\text{Ru}_6\text{S}_6$): 1,112.74 [**9**- $3\text{CF}_3\text{SO}_3$] $^{3+}$.

Synthesis of the metalla-prismatic cage **10**

A mixture of tripodal donor **4** (3.0 mg, 0.008 mmol), ruthenium acceptor **2** (11.4 mg, 0.012 mmol) and guest molecule ellagic acid (1.2 mg, 0.004 mmol) in $\text{CH}_3\text{OH}/\text{CH}_3\text{NO}_2$ (2 mL, 1:1) was stirred at 40°C for 24 hours. The reaction mixture was then filtered and concentrated by using a rotavapor to reduce the volume followed by the addition of diethyl ether which yielded **10** as a sea-green powder. Yield 90%; ^1H NMR (300 MHz, $\text{CD}_3\text{NO}_2:\text{CD}_3\text{OD}$ [1:1] solution, ppm): δ 8.46 (d, $J=6.8$ Hz, 12H), 7.45 (s, 2H), 7.41 (d, $J=5.0$ Hz, 12H), 7.29 (s, 12H), 7.03 (s, 6H), 5.78 (d, $J=6.0$ Hz, 12H), 5.57 (d, $J=6.1$ Hz, 12H), 2.87 (d, $J=6.7$ Hz, 6H), 2.13 (s, 18H), 1.34 (d, $J=6.8$ Hz, 36H); MS (ESI) for **10** ($\text{C}_{164}\text{H}_{132}\text{F}_{18}\text{N}_6\text{O}_{38}\text{Ru}_6\text{S}_6$): 1,162.74 [**10**- $3\text{CF}_3\text{SO}_3$] $^{3+}$.

Synthesis of the metalla-prismatic cage **11**

A mixture of tripodal donor **4** (3.0 mg, 0.008 mmol), ruthenium acceptor **3** (12.6 mg, 0.012 mmol) and guest molecule ellagic acid (1.2 mg, 0.004 mmol) in $\text{CH}_3\text{OH}/\text{CH}_3\text{NO}_2$ (2 mL, 1:1) was stirred at 40°C for 24 hours. The reaction mixture was then filtered and concentrated by using a rotavapor to reduce the volume followed by the addition of diethyl ether which yielded **11** as a green crystalline solid. Yield 87%; ^1H NMR (300 MHz, nitromethane:MeOD [1:1] solution, ppm): δ 8.77 (dd, $J=6.0$, 3.4 Hz, 12H), 8.53 (d, $J=6.4$ Hz, 12H), 7.99 (dd, $J=6.0$, 3.4 Hz, 12H), 7.27 (d, $J=6.4$ Hz, 14H), 6.77 (s, 6H), 5.97 (d, $J=6.3$ Hz, 12H), 5.74 (d, $J=6.3$ Hz, 12H), 3.07–2.96 (m, $J=6.9$ Hz, 6H), 2.23 (s, 18H), 1.36 (d, $J=6.9$ Hz, 36H); MS (ESI) for **11** ($\text{C}_{188}\text{H}_{144}\text{F}_{18}\text{N}_6\text{O}_{38}\text{Ru}_6\text{S}_6$): 1,262.78 [**11**- $3\text{CF}_3\text{SO}_3$] $^{3+}$.

Statistical analysis

All quantitative results were expressed as mean \pm standard error (SE). Statistical analysis was performed using Student's *t*-test. Values of $P < 0.05$ and $P < 0.01$ were considered to be statistically significant.

Results and discussion

Syntheses of the empty metalla-prisms **6**, **7**, and **8** have been reported previously.¹⁴ Ellagic acid (**5**) encapsulated in metalla-prisms **9**, **10**, and **11** were readily prepared

quantitatively by the reaction of one of the binuclear $[\text{Ru}_2(p\text{-}i\text{PrC}_6\text{H}_4\text{Me})_2(\text{dobq})(\text{MeOH})_2][\text{CF}_3\text{SO}_3]_2$ **1**,⁴⁰ $[\text{Ru}_2(p\text{-}i\text{PrC}_6\text{H}_4\text{Me})_2(\text{donq})(\text{H}_2\text{O})_2][\text{CF}_3\text{SO}_3]_2$ **2**,⁴¹ or $[\text{Ru}_2(p\text{-}i\text{PrC}_6\text{H}_4\text{Me})_2(\text{dotq})][\text{CF}_3\text{SO}_3]_2$ **3**¹⁴ acceptors with the tripyridyl donor **4**⁴² and ellagic acid (**5**) in a 3:2:1 ratio (Figure 1). The addition of diethyl ether to the concentrated reaction mixtures resulted in the isolation of analytically pure hexanuclear cages as crystalline solids. All the cages were fully characterized by ^1H NMR, electrospray ionization mass spectrometry, and UV/Vis absorption.

The formation of the compounds **9–11** was monitored by ^1H NMR spectroscopy in $\text{CD}_3\text{NO}_2:\text{CD}_3\text{OD}$ solution (1:1, Figure 2). The resonance of the ellagic acid proton was observed to be shifted upfield upon formation of the encapsulated system compounds **9–11**. Similarly, in the ^1H NMR spectra of **9–11**, the signals corresponding to the H_α and H_β nuclei of the pyridine rings were observed to undergo upfield shifts ($\Delta\delta=0.2\text{--}0.3$ ppm) relative to **4**, indicative of the metal pyridine coordination. Protons of the ligand panel in **9–11** were shifted upfield in comparison with the empty cages **6–8**. The signals of the *CH* protons of the *dobq*, *donq*, and *dotq* bridging ligands remained almost unchanged. The proton resonances of the *p*-cymene ligands located at the periphery of the prism were not significantly affected by the presence of ellagic acid (**5**) in the cavities of **9–11**.

Diffusion-ordered NMR spectroscopy^{43–45} confirms the encapsulation of ellagic acid into the cavity of **10** (Figures S1–S4). The diffusion-ordered NMR spectroscopy measurement of the empty cage **7** and the inclusion system **10** gave diffusion coefficients (*D*) of $6.1 \times 10^{-10} \text{ m}^2 \cdot \text{s}^{-1}$ and $5.6 \times 10^{-10} \text{ m}^2 \cdot \text{s}^{-1}$, respectively.

Electrospray ionization mass spectrometry (ESI-MS) analysis confirmed the formation of [3+2] self-assembled hexanuclear cages **9–11** encapsulating ellagic acid, by the appearance of multiple-charged fragments. The multiple-charged ions were observed: for **9** at $m/z=1,112.7$ [**9**- $3\text{CF}_3\text{SO}_3$] $^{3+}$, for **10** at $m/z=1,163.06$ [**10**- $3\text{CF}_3\text{SO}_3$] $^{3+}$ and for **11** at $m/z=1,263.11$ [**11**- $3\text{CF}_3\text{SO}_3$] $^{3+}$ and these peaks were well resolved isotopically (Figure 3). The appearance of the expected peaks, together with the isotopic patterns, confirmed the formation of the expected ellagic acid-encapsulated self-assembled products **9–11**.

UV/Vis absorption spectra

The UV/Vis absorption spectra of **6–11** and ellagic acid (**5**) were also investigated (Figure 4). High-energy bands were observed in the spectra of **6–11**, and the absorbance

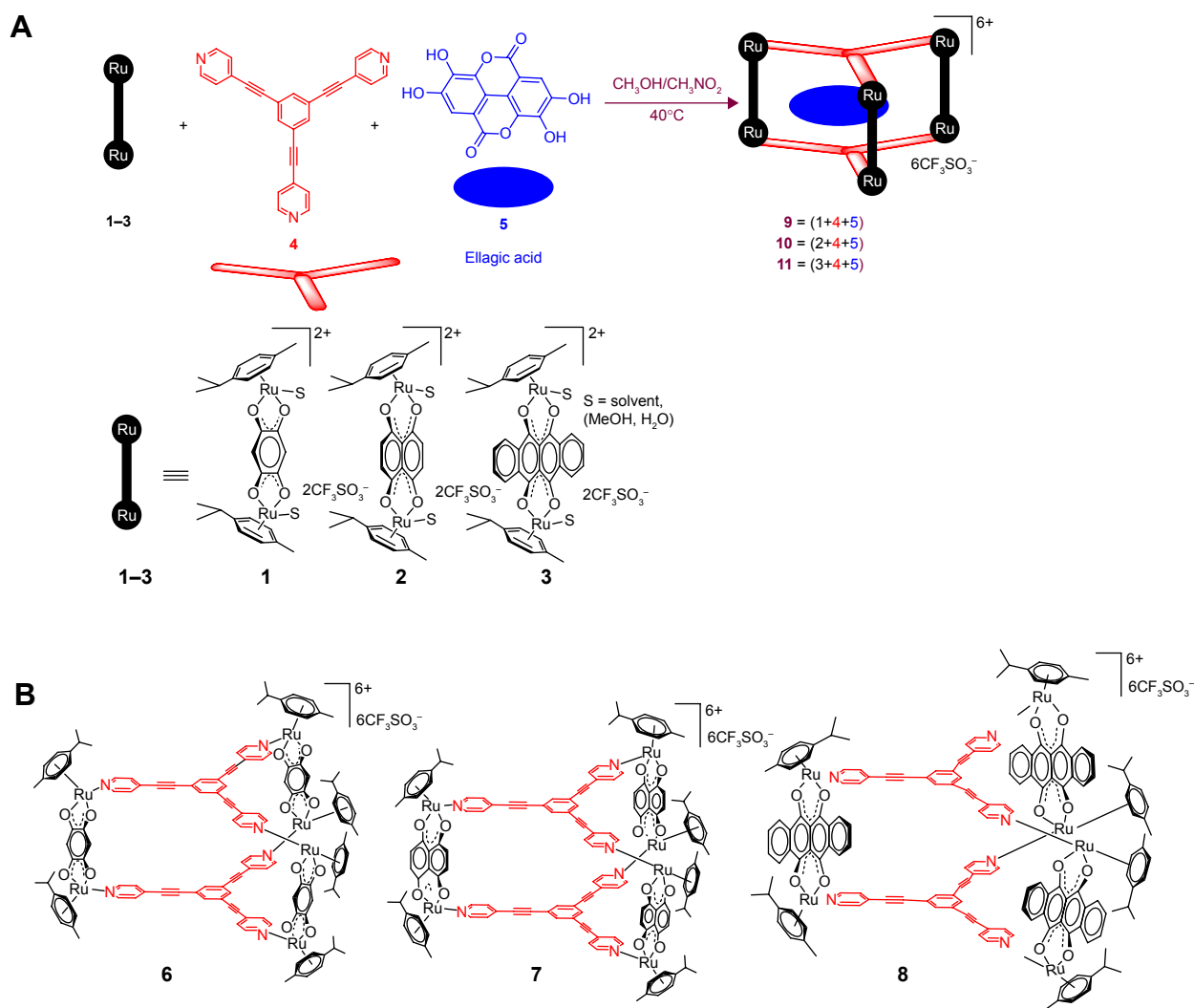


Figure 1 (A) Synthesis of ellagic acid-encapsulated arene-ruthenium metalla-prisms **9–11** and (B) arene-ruthenium metalla-prisms **6–8**.

bands of **8** and **11** were dominated by $\pi \rightarrow \pi^*$ transitions of the tetracene moieties from 550 nm to 620 nm. A significant hypochromic effect observed in the spectra of complexes **9** and **10**, in comparison with **7** and **8** was due to the distortion of the geometry by the encapsulation of ellagic acid (**5**).

Antioxidant activity

Reactive oxygen species and the resultant oxidative damage have been implicated in pathogenesis and there is scientific evidence to suggest that antioxidants reduce the risk of chronic conditions including cancer and heart disease.^{46–48} In this study, the antioxidant activities of the prepared compounds were evaluated by the ORAC assay. Compounds **9** and **10** showed potent antioxidant activity with **10** having the most significant level of activity of all the tested compounds, with an ORAC_{PE} value of 1.30 ± 0.020 . In contrast,

ellagic acid (**5**) and compound **11** showed weaker activity than Trolox (Table 1).

Effects of cancer cell growth inhibition

Organometallic arene-Ru-based half-sandwich complexes have attracted interest as potential anticancer agents due to their activity against a range of cancer cells accompanied by low toxicity and lack of cross-resistance with cisplatin. The cytotoxicity of ellagic acid (**5**) and encapsulated cages **9–11** was explored in vitro using the human cancer cell lines: SK-hep-1 (liver cancer), AGS (gastric cancer), and A549 (lung cancer). These cell lines were exposed to increasing concentrations of the test compounds for 24 hours, after which a colorimetric MTT assay was performed. The results, summarized in Table 2, were compared with those determined for the well-known anticancer drug, doxorubicin. Ellagic acid (**5**) and cages **9** and **11** displayed poor activity.

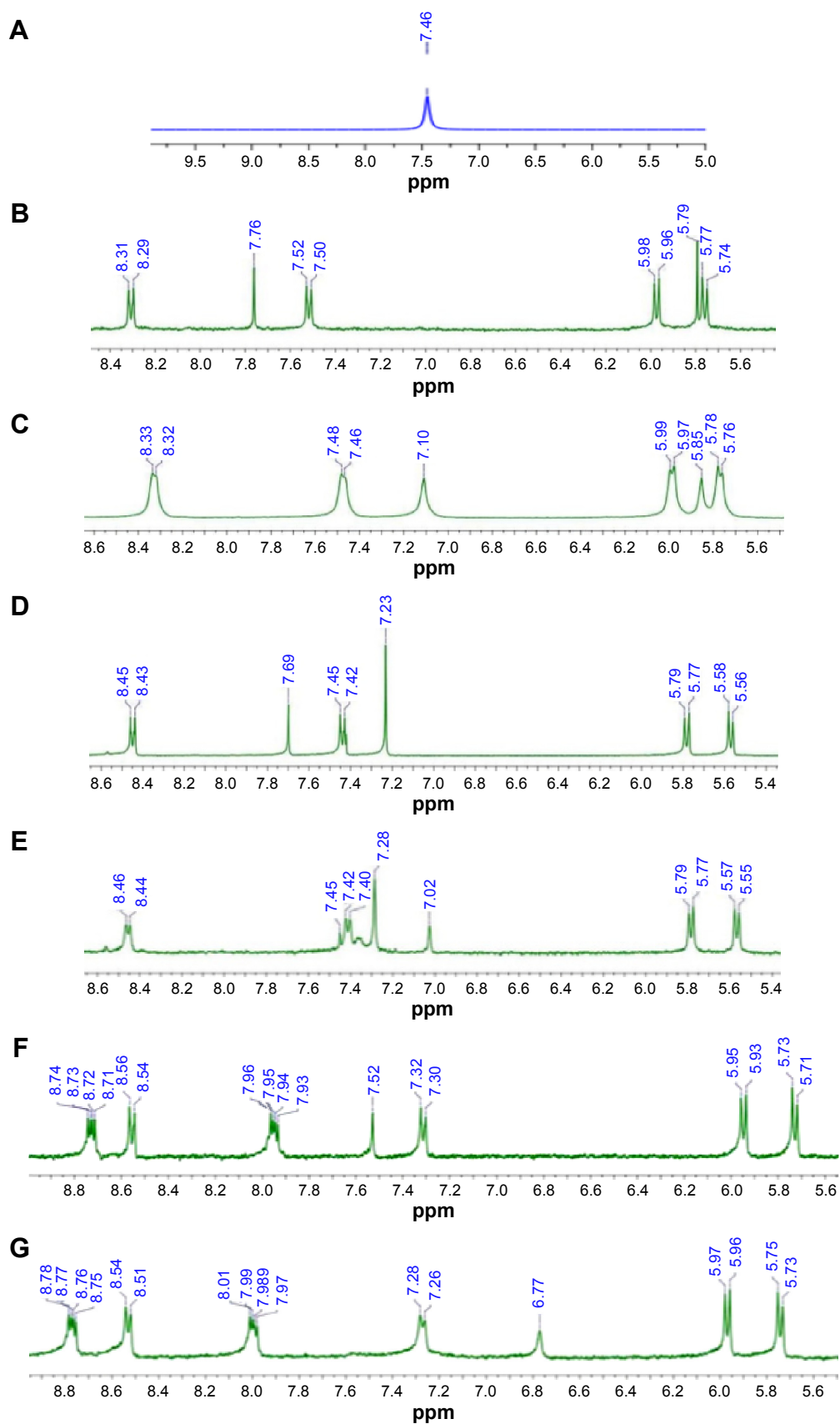


Figure 2 Excerpts of ^1H NMR spectra of (A) ellagic acid (5), (B) empty prism 6, (C) encapsulated prism 9, (D) empty prism 7, (E) encapsulated prism 10, (F) empty prism 8 and (G) encapsulated prism 11 in $\text{CD}_3\text{NO}_2:\text{CD}_3\text{OD}$ (1:1) solution.

Abbreviation: ppm, parts per million.

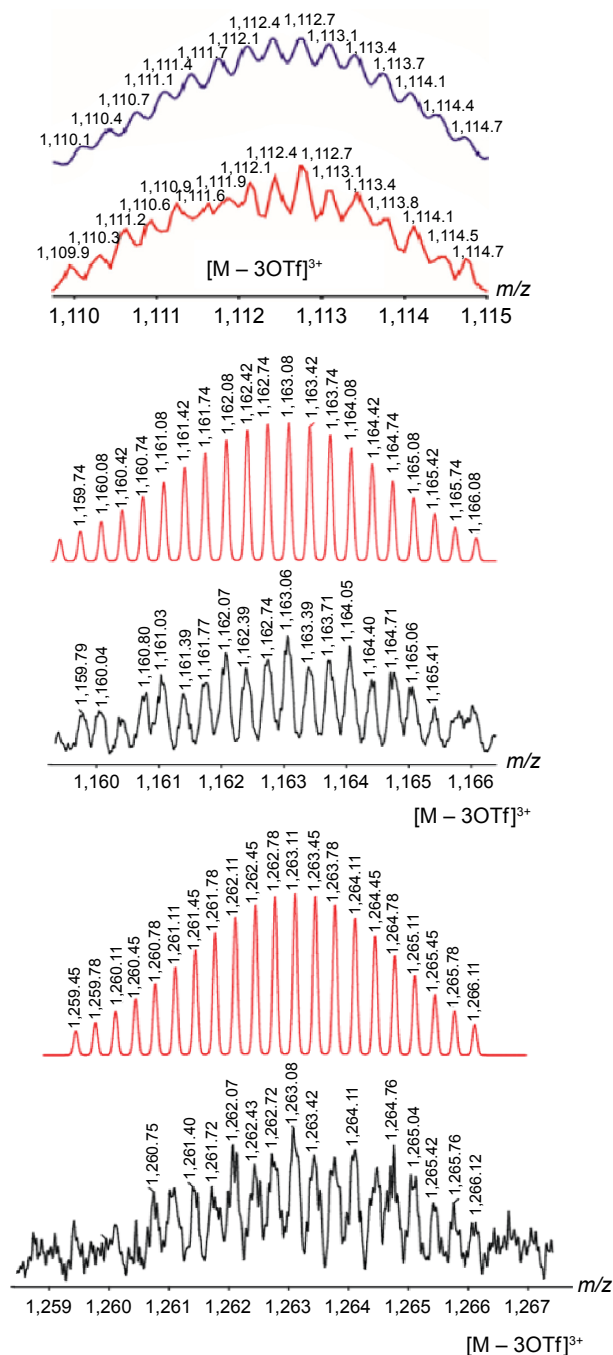


Figure 3 Calculated (red) and experimental (black) ESI-MS spectra of ellagic acid encapsulated prisms 9–11.

Abbreviation: ESI-MS, electrospray ionisation mass spectrometry.

However, compound **10** exhibited inhibition against all cancer cell lines at low micromolar concentrations, with the highest cytotoxicity against the A549 human lung cancer cell line ($IC_{50} = 25.9 \mu\text{M}$). Zahin et al demonstrated that ellagic acid decreased cell survival rates of A549 cells to 61% at a concentration of $165 \mu\text{M}$, suggesting that the encapsulation of ellagic acid in nano-sized metalla-prisms increased the anticancer efficacy of ellagic acid.⁴⁹

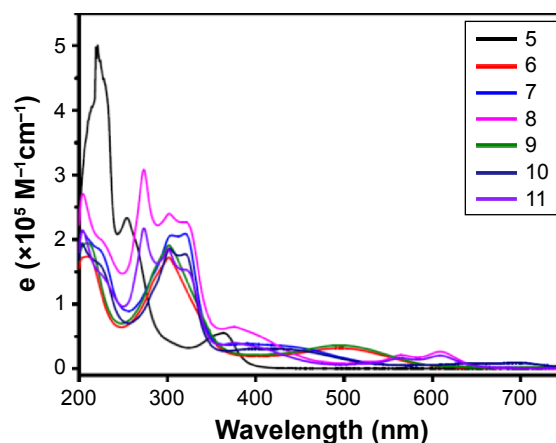


Figure 4 UV/Vis spectra of ellagic acid (**5**), empty metalla-prisms **6–8** and ellagic acid-encapsulated metalla-prisms **9–11** in a solution of methanol ($1 \times 10^{-5} \text{ M}$).

Abbreviation: UV/Vis, ultraviolet/visible.

Macrophage-mediated tumoricidal activity

Cells of the monocyte–macrophage lineage have the capacity to recognize and destroy tumor cells^{50,51} when activated by lymphokines such as IFN- γ and G-CSF.^{52,53} In this study, macrophages were pretreated with the test materials (ellagic acid [**5**] and cage **10**) or the control medium, before being co-cultured with B16/F10 cells to assess the ability of the compounds to activate macrophages to kill tumor cells. Figure 5A indicated that ellagic acid and compound **10** did not exert cytotoxic effects but doxorubicin did in B16/F10 mouse skin carcinoma when these were incubated without macrophages. Figure 5B showed that ellagic acid and compound **10** incubated with macrophages kill 55.1% (at $2 \mu\text{M}$ of ellagic acid) and 58.6% (at $2 \mu\text{M}$ of compound **10**) of cancer cells compared to the untreated macrophages with B16/F10 cells whereas doxorubicin was less effective compared to its effect without macrophages. Therefore, ellagic acid and compound **10** are macrophage-dependent in terms of their cytotoxicity against cancer cells.

Table 1 Anti-oxidative effects of ellagic acid (**5**) and cage compounds **9–11**

Compound	Molecular weight	ORAC _{PE} values
Ellagic acid (5)	302.19	0.65 ± 0.029^a
6	3,483.23	<0.5
7	3,633.41	<0.5
8	3,933.76	<0.5
9	3,785.43	1.23 ± 0.023^a
10	3,935.60	1.30 ± 0.020^a
11	4,235.95	0.93 ± 0.014^a

Notes: Trolox (vitamin E) ORAC_{PE} value 1. ^aValues are mean \pm SE.

Abbreviations: ORAC, oxygen-radical absorbance capacity; SE, standard error.

Table 2 Inhibition effects on cell viability after exposure of human cancer cell lines to ellagic acid (5), compounds 9–11 and Doxorubicin

Compound	IC ₅₀ (μM) ^a		
	SK-hep-1	AGS	A549
Ellagic acid (5)	>200	>200	>200
6	>200	>200	>200
7	>200	>200	>200
8	>200	>200	>200
9	>200	>200	>200
10	86.6±1.17	88.2±2.64	25.9±2.40
11	187.1±6.17	>200	>200
Doxorubicin ^b	3.02±0.18	2.14±0.10	3.18±0.09

Notes: ^aIC₅₀ is the drug concentration necessary for 50% inhibition of cell viability. Data are shown as mean ± SE. ^bDoxorubicin (positive control) was used as itself.

Abbreviation: SE, standard error.

Cytokine secretion

Cytokines are signaling molecules that play critical roles in many biological processes such as cellular growth, differentiation, gene expression, migration, immunity, and inflammation. Macrophages release cytokines to activate and recruit other cells during inflammation, or as direct killing agents.^{54,55} The co-incubation of activated macrophages with tumor cells either up- or down-regulated the production of different cytokines depending on the nature of the tumor cells, thereby modulating the susceptibility of these tumor cells to macrophage-mediated tumor cytotoxicity.⁵⁶ We measured the effect of ellagic acid and compound 10 on the secretion of 23 cytokines by using macrophages, with an enzyme-linked immunosorbent assay (ELISA) array chosen to represent cytokines, which are known to inhibit the growth of tumor cells. As shown in Figure 6, compound 10 stimulated G-CSF by 18.4% compared to control cells. G-CSF decreases the morbidity of cancer chemotherapy by reducing the incidence

of febrile neutropenia.⁵⁷ However, treatment with ellagic acid actually inhibited G-CSF secretion using macrophages. In contrast, macrophages treated with ellagic acid showed a 26.9% increased secretion of IFN-γ which stimulates several anti-proliferative and thus tumoricidal biochemical pathways in macrophages as well as in tumor cell lines.^{58–60} In addition, compound 10 reduced Rantes secretion from macrophages (–43.2%) in contrast, to the increase (11.1%) seen with ellagic acid. Rantes is highly expressed in various tumors and promotes tumor growth and metastasis by inducing tumor cell proliferation and angiogenesis.^{61–63} In summary, macrophages treated with compound 10 may inhibit the growth of cancer cells due to the increased secretion of G-CSF and decreased secretion of Rantes.

Molecular ligand mRNA expression of macrophages

The inhibition of tumor cell growth exerted by compound 10 was apparently through the modulation of a different set of macrophage proteins than those affected by the naked ellagic acid. While ellagic acid encapsulated in compound 10 acted on G-CSF and Rantes, the naked ellagic acid had an effect on IFN-γ secretion or protein expression (Figure 6). In order to confirm these results, we investigated the mRNA expression of G-CSF and Rantes in the macrophage RAW264.7 cell line by using the real-time polymerase chain reaction. G-CSF was increased by compound 10 (~2.1 times vs control) and Rantes was decreased (~0.4 times vs control) with respect to the mRNA levels (Figure 7). These results demonstrate that ellagic acid encapsulated into a nano-sized metalla-cage inhibited tumor cells through the modulation of G-CSF and Rantes in macrophages at the level of both protein and mRNA.

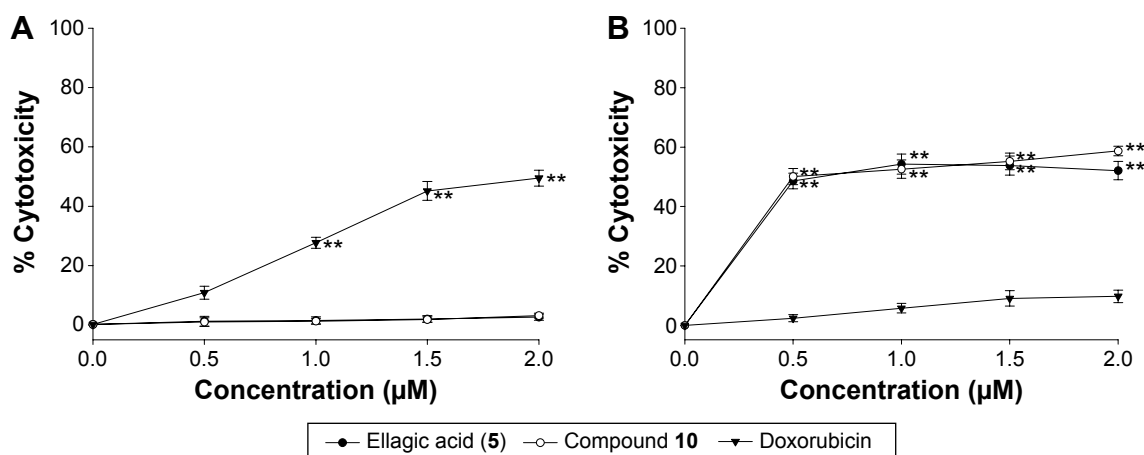


Figure 5 Tumoricidal effects of ellagic acid (5) and compound 10 on co-cultured B16/F10 mouse skin carcinoma and RAW264.7 mouse macrophage cells. (A) Ellagic acid (5) and compound 10 without macrophage pretreatment. (B) Elicited macrophages pretreated with ellagic acid (5) and compound 10 24 hours before incubation with B16 cells.

Notes: The results are mean ± SE of triplicates from a representative experiment. ***P*<0.01; significantly different from the control.

Abbreviation: SE, standard error.

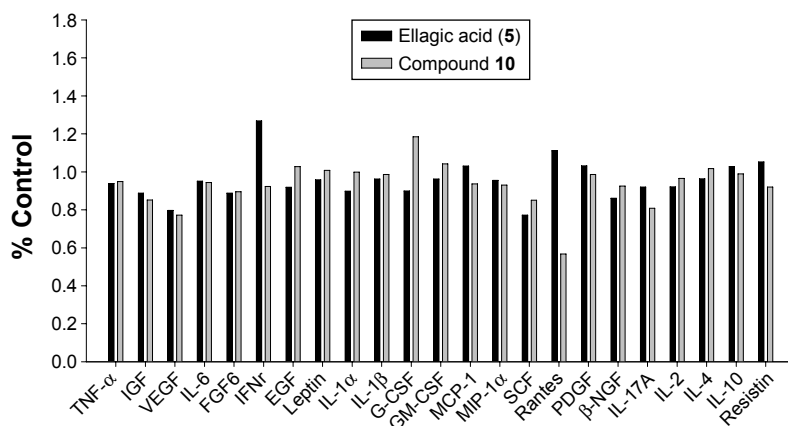


Figure 6 Plot showing the change in cytokine secretion of RAW264.7 macrophages with ellagic acid and compound 10.

Abbreviations: TNF- α , tumor necrosis factor alpha; IGF, insulin-like growth factor; VEGF, vascular endothelial growth factor; IL-6, interleukin-6; FGF6, fibroblast growth factor 6; IFN γ , interferon gamma; EGF, epidermal growth factor; IL-1 α , interleukin-1 alpha; IL-1 β , interleukin-1 beta; G-CSF, granulocyte-colony stimulating factor; GM-CSF, granulocyte-macrophage colony-stimulating factor; MCP-1, monocyte chemoattractant protein-1; MIP-1 α , macrophage inflammatory protein-1 alpha; SCF, cullin, F-box-containing complex; Rantes, regulated on activation, normal T cell expressed and secreted; PDGF, platelet-derived growth factor; β -NGF, beta-nerve growth factor; IL-17A, interleukin-17A; IL-2, interleukin-2; IL-4, interleukin-4; IL-10, interleukin-10.

Conclusion

We have described the synthesis, characterization, host-guest properties, antioxidant and anti-cancer activity of ellagic acid-encapsulated Ru-based nano-prismatic cages. Our antioxidant studies of these complexes reveal that complexes 9 and 10 have antioxidant activity superior to Trolox, a derivative of vitamin E which has been used as an

adjunctive therapeutic agent for certain cancers. Nanotechnology approaches, including the encapsulation of synthesized or natural products into biocompatible nanoparticles or nano-sized materials, were initially applied to cancer therapeutics to decrease toxicity, increase bioavailability, and promote the selectivity of the tumor. Our results in this study indicate that compound 10 inhibited the A549 human

Ellagic acid encapsulated metalla-cage (10)

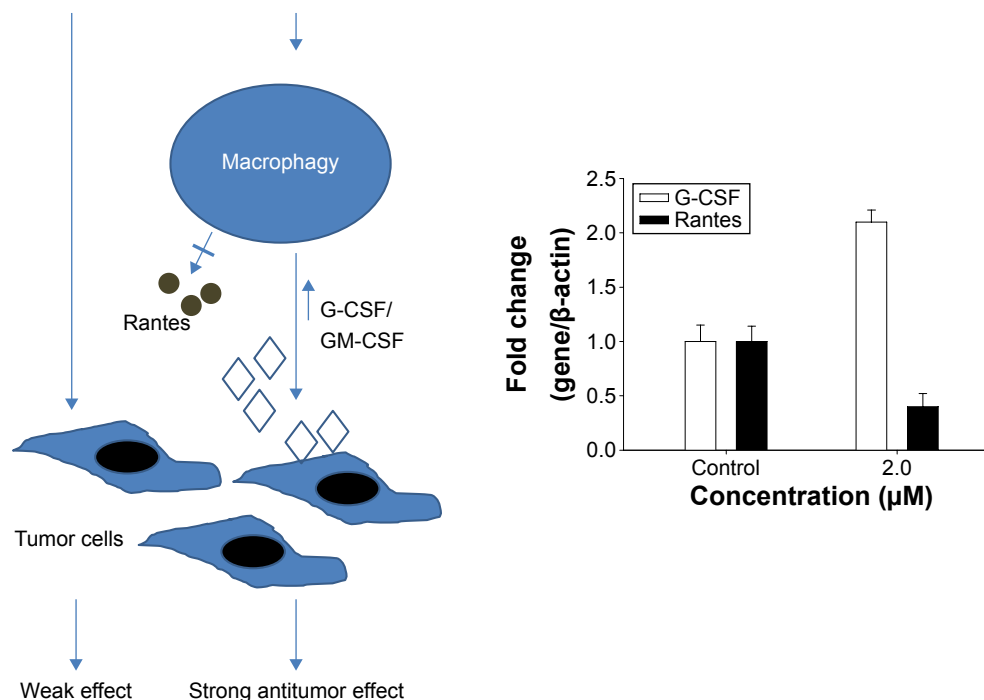


Figure 7 Schematic representing the proposed events and G-CSF and Rantes gene expression in RAW264.7 macrophages with ellagic acid (control) and compound 10.

Notes: The upward arrows indicate an increase in the G-CSF level and the crossed arrow indicates the inhibition of Rantes.

Abbreviations: Rantes, regulated on activation normal T cell expressed and secreted; G-CSF, granulocyte-colony stimulating factor.

lung cancer cell line, whereas the free ellagic acid itself lacked activity. In a tumoricidal assay system, ellagic acid as well as complex **10** inhibited the growth of tumor cells while doxorubicin lacked activity. At the same time, IFN γ was induced by ellagic acid while compound **10** had no effect on IFN γ , but did stimulate G-CSF and inhibit Rantes in RAW264.7 macrophage cell ligand expression where ellagic acid had no effect. Our results show that ellagic acid-encapsulated metalla-cage **10**, exhibited an inhibitory effect for cancer cells via G-CSF induction and Rantes inhibition in macrophages at both mRNA and protein levels. This study serves as the first step toward establishing ellagic acid encapsulated into nano-sized metalla-cages as promising anticancer therapeutic agents, superior to the existing chemopreventative agents.

Acknowledgment

This work was supported by the 2015 Research Fund of the University of Ulsan.

Disclosure

The authors report no conflicts of interest in this work.

References

- Zhu J, Wang XZ, Chen YQ, Jiang XK, Chen XZ, Li ZT. Hydrogen-bonding-induced planar, rigid, and zigzag oligoanthranilamides. Synthesis, characterization, and self-assembly of a metallocyclophane. *J Org Chem*. 2004;69:6221–6227.
- Amouri H, Desmarts C, Moussa J. Confined nanospaces in metal-locages: guest molecules, weakly encapsulated anions, and catalyst sequestration. *Chem Rev*. 2012;112:2015–2041.
- Koblenz TS, Wassenaar J, Joost Reek JNH. Reactivity within a confined self-assembled nanospace. *Chem Soc Rev*. 2008;37:247–262.
- Breiner B, Clegg JK, Jonathan R, Nitschke JR. Reactivity modulation in container molecules. *Chem Sci*. 2011;2:51–56.
- Fiedler D, Leung DH, Bergman RG, Raymond KN. Selective molecular recognition, C–H bond activation, and catalysis in nanoscale reaction vessels. *Acc Chem Res*. 2005;38:349–358.
- Yoshizawa M, Klosterman JK, Fujita M. Functional molecular flasks: new properties and reactions within discrete, self-assembled hosts. *Angew Chem Int Ed*. 2009;48:3418–3438.
- Flamigni L, Ventura B, Oliva AI, Ballester P. Energy migration in a self-assembled nonameric porphyrinic molecular box. *Chemistry*. 2008;14:4214–4224.
- Indelli MT, Chiorboli C, Scandola F, Iengo E, Osswald P, Wurthner F. Photoinduced processes in self-assembled porphyrin/perylene bisimide metallosupramolecular boxes. *J Phys Chem B*. 2010;114:14495–14504.
- Sprafke JK, Kondratuk DV, Wykes M, et al. Belt-shaped π -systems: relating geometry to electronic structure in a six-porphyrin nanoring. *J Am Chem Soc*. 2011;133:17262–17273.
- Cook TR, Vajpayee V, Lee MH, Stang PJ, Chi KW. Biomedical and biochemical applications of self-assembled metallacycles and metal-lacages. *Acc Chem Res*. 2013;46:2464–2474.
- Ahmad N, Younus HA, Chughtai AH, Verpoort F. Metal–organic molecular cages: applications of biochemical implications. *Chem Soc Rev*. 2015;44:9–25.
- Therrien B. Transporting and shielding photosensitizers by using water-soluble organometallic cages: a new strategy in drug delivery and photodynamic therapy. *Chemistry*. 2013;19:8378–8386.
- Hannon MJ, Moreno V, Prieto MJ, et al. Intramolecular DNA coiling mediated by a metallo-supramolecular cylinder. *Angew Chem Int Ed Engl*. 2001;40:879–884.
- Vajpayee V, Yang YJ, Kang SC, et al. Hexanuclear self-assembled arene-ruthenium nano-prismatic cages: potential anticancer agents. *Chem Commun*. 2011;47:5184–5186.
- Dubey A, Min JK, Hyun Koo HJ, et al. Anticancer potency and multi drug resistant studies of self-assembled arene-ruthenium metallarectangles. *Chemistry*. 2013;19:11622–11628.
- Vajpayee V, Song YH, Jung YJ, et al. Coordination-driven self-assembly of ruthenium-based molecular-rectangles: synthesis, characterization, photophysical and anticancer potency studies. *Dalton Trans*. 2012;41:3046–3052.
- Mishra A, Ravikumar S, Hong SH, et al. DNA binding and unwinding by self-assembled supramolecular hetero-bimetallic cycles. *Organometallics*. 2011;30:6343–6346.
- Jung H, Dubey A, Koo HJ, et al. Self-assembly of ambidentate pyridyl-carboxylate ligands with octahedral ruthenium metal center: self-selection for a single-linkage isomer and anticancer-potency studies. *Chemistry*. 2013;19:6709–6717.
- Vajpayee V, Lee SM, Park JW, et al. Growth inhibitory activity of a bis-benzimidazole-bridged arene ruthenium metalla-rectangle and prism. *Organometallics*. 2013;32:1563–1566.
- Chakrabarty R, Mukherjee PS, Stang PJ. Supramolecular coordination: self-assembly of finite two- and three-dimensional ensembles. *Chem Rev*. 2011;111:6810–6918.
- Cook TR, Zheng YR, Stang PJ. Metal–organic frameworks and self-assembled supramolecular coordination complexes: comparing and contrasting the design, synthesis, and functionality of metal–organic materials. *Chem Rev*. 2013;113:734–777.
- Vallet-Regi M, Balas F, Arcos D. Mesoporous materials for drug delivery. *Angew Chem Int Ed Engl*. 2007;46:7548–7558.
- Gabano E, Ravera M, Osella D. The drug targeting and delivery approach applied to pt-antitumour complexes. A coordination point of view. *Curr Med Chem*. 2009;16:4544–4580.
- Dyson PJ, Sava G. Metal-based antitumour drugs in the post genomic era. *Dalton Trans*. 2006;16:1929–1933.
- van Rijt SH, Sadler PJ. Current applications and future potential for bioinorganic chemistry in the development of anticancer drugs. *Drug Discov Today*. 2009;14:1089–1097.
- Sanchez-Cano C, Hannon MJ. Novel and emerging approaches for the delivery of metallo-drugs. *Dalton Trans*. 2009;48:10702–10711.
- Boulvikas T, Vougiouka M. Cisplatin and platinum drugs at the molecular level. (Review). *Oncol Rep*. 2003;10:1663–1682.
- Lovejoy KS, Lippard SJ. Non-traditional platinum compounds for improved accumulation, oral bioavailability, and tumor targeting. *Dalton Trans*. 2009;48:10651–10659.
- van der Vlugt JI, Koblenz TS, Wassenaar J, Reek JNH. Chapter 6. Chemistry in self-assembled nanoreactor. In: Brinker UH, Miesusset J-L, editors. *Molecular Encapsulation: Organic Reactions in Constrained Systems*. New York: Wiley; 2010:145–174.
- Brantley EC, Guo L, Zhang C, et al. Nitric oxide-mediated tumoricidal activity of murine microglial cells. *Transl Oncol*. 2010;3:380–388.
- Mantovani A, Garlanda C, Allavena P. Molecular pathways and targets in cancer-related inflammation. *Ann Med*. 2010;42:161–170.
- Wanda L, Ou B. Antioxidant activity and phenolic content of Oregon caneberries. *J Agric Food Chem*. 2002;50:3495–3500.
- Zhang HM, Zhao L, Li H, Xu H, Chen WW, Tao L. Research progress on the anticarcinogenic actions and mechanisms of ellagic acid. *Cancer Biol Med*. 2014;11:92–100.
- Teel RW, Martin RM. Disposition of the plant phenol ellagic acid in the mouse following oral administration by gavage. *Xenobiotica*. 1988;18:397–405.

35. Smart RC, Huang MT, Chang RL, Sayer JM, Jerina DM, Conney AH. Disposition of the naturally occurring antimutagenic plant phenol, ellagic acid, and its synthetic derivatives, 3-O-decylellagic acid and 3,3'-di-O-methylellagic acid in mice. *Carcinogenesis*. 1986;7:1663–1667.
36. Shirole AB, Bharali DJ, Nallanthighal S, Coon JK, Mousa SA, Reliene R. Nanoencapsulation of pomegranate bioactive compounds for breast cancer chemoprevention. *Int J Nanomedicine*. 2015;10:475–484.
37. Gillespie KM, Chae JM, Ainsworth EA. Rapid measurement of total antioxidant capacity in plants. *Nat Protoc*. 2007;2:867–870.
38. Ou B, Hampsch-Woodill M, Prior RL. Development and validation of an improved oxygen radical absorbance capacity assay using fluorescein as the fluorescent probe. *J Agric Food Chem*. 2001;49:4619–4626.
39. Ghaffar A, Cullen R, Woodruff M. Further analysis of the anti-tumour effect in vitro of peritoneal exudate cells from mice treated with *Corynebacterium parvum*. *Br J Cancer*. 1975;31:15–24.
40. Therrien B, Süss-Fink G, Govindaswamy P, Renfrew AK, Dyson PJ. The “complex-in-a-complex” cations [(acac)₂M subset Ru₆(p-iPrC₆H₄Me)₆(tpt)₂(dhbq)₃]⁶⁺: a Trojan horse for cancer cells. *Angew Chem Int Ed Engl*. 2008;47:3773–3776.
41. Pitto-Barry A, Barry NP, Zava O, Deschenaux R, Therrien B. Double targeting of tumours with pyrenyl-modified dendrimers encapsulated in an arene-ruthenium metallaprism. *Chem Asian J*. 2011;17:1966–1971.
42. Norifumi K, Masashi K. 1,3,5-tris(functionalised-phenylethynyl) benzene-metal complexes: synthetic survey of mesoporous coordination polymers and investigation of their carbonisation. *J Mater Chem*. 2008;18:1037–1045.
43. Wu DH, Chen A, Johnson CS. Flow imaging by means of 1D pulsed-field-gradient NMR with application to electroosmotic flow. *J Magn Reson A*. 1995;115:123–126.
44. Johnson CS. Diffusion ordered nuclear magnetic resonance spectroscopy: principles and applications. *Prog Nucl Magn Reson Spectrosc*. 1999;34:203–256.
45. Barry NPE, Furrer J, Freudenreich J, Süss-Fink G, Therrien B. Designing the host-guest properties of tetranuclear arene ruthenium metalla-rectangles to accommodate a pyrene molecule. *Eur J Inorg Chem*. 2010;2010:725–728.
46. Ames BN, Gold LS, Willett WC. The causes and prevention of cancer. *Proc Natl Acad Sci U S A*. 1995;92:5258–5265.
47. Favier AE, Cadet J, Kalyanaraman B, Fontecave M, Pierre JL. *Analysis of Free Radicals in Biological Systems*. 1st ed. Basel: Birkhauser; 1995:83–98.
48. Witztum JL. The oxidation hypothesis of atherosclerosis. *Lancet*. 1994;344:793–795.
49. Zahin M, Ahmad I, Gupta R, Aqil F. Punicalagin and ellagic acid demonstrate antimutagenic activity and inhibition of benzo[a]pyrene induced DNA adducts. *Biomed Res Int*. 2014;2014:467465.
50. Klimp AH, de Vries EG, Scherphof GL, Daemen T. A potential role of macrophage activation in the treatment of cancer. *Crit Rev Oncol Hematol*. 2002;44:143–161.
51. Bingle L, Brown NJ, Lewis CE. The role of tumor-associated macrophages in tumour progression: implications for new anticancer therapies. *J Pathol*. 2002;196:254–265.
52. Schultz RM, Kleinschmidt WJ. Functional identity between murine gamma interferon and macrophage activating factor. *Nature*. 1983;305:239–240.
53. Zahedi K, Mortensen RF. Macrophage tumoricidal activity induced by human C-reactive protein. *Cancer Res*. 1986;46:5077–5083.
54. Holgate ST. The role of mast cells and basophils in inflammation. *Clin Exp Allergy*. 2000;1:28–32.
55. Hume DA. The mononuclear phagocyte system. *Curr Opin Immunol*. 2006;18:49–53.
56. Song JY, Han SK, Son EH, Pyo SN, Yun YS, Yi SY. Induction of secretory and tumoricidal activities in peritoneal macrophages by ginsan. *Int Immunopharmacol*. 2002;2:857–865.
57. Crawford J, Ozer H, Stoller R, et al. Reduction by granulocyte colony-stimulating factor of fever and neutropenia induced by chemotherapy in patients with small-cell lung cancer. *N Engl J Med*. 1991;325:164–170.
58. Brandacher G, Winkler C, Schroecksnadel K, Margreiter R, Fuchs D. Antitumoral activity of interferon-gamma involved in impaired immune function in cancer patients. *Curr Drug Metab*. 2006;7:599–612.
59. Lanier LL. NK cell receptors. *Annu Rev Immunol*. 1998;16:359–393.
60. Diefenbach A, Raulet DH. The innate immune response to tumors and its role in the induction of T-cell immunity. *Immunol Rev*. 2002;188:9–21.
61. Mrowietz U, Schwenk U, Maune S, et al. The chemokine RANTES is secreted by human melanoma cells and is associated with enhanced tumour formation in nude mice. *Br J Cancer*. 1999;79:1025–1031.
62. Sugawara H, Ichikura T, Kinoshita M, et al. Gastric cancer cells exploit CD4+ cell-derived CCL5 for their growth and prevention of CD8+ cell-involved tumor elimination. *Int J Cancer*. 2008;122:2531–2541.
63. Soria G, Ben-Baruch A. The inflammatory chemokines CCL2 and CCL5 in breast cancer. *Cancer Lett*. 2008;267:271–285.

Supplementary materials

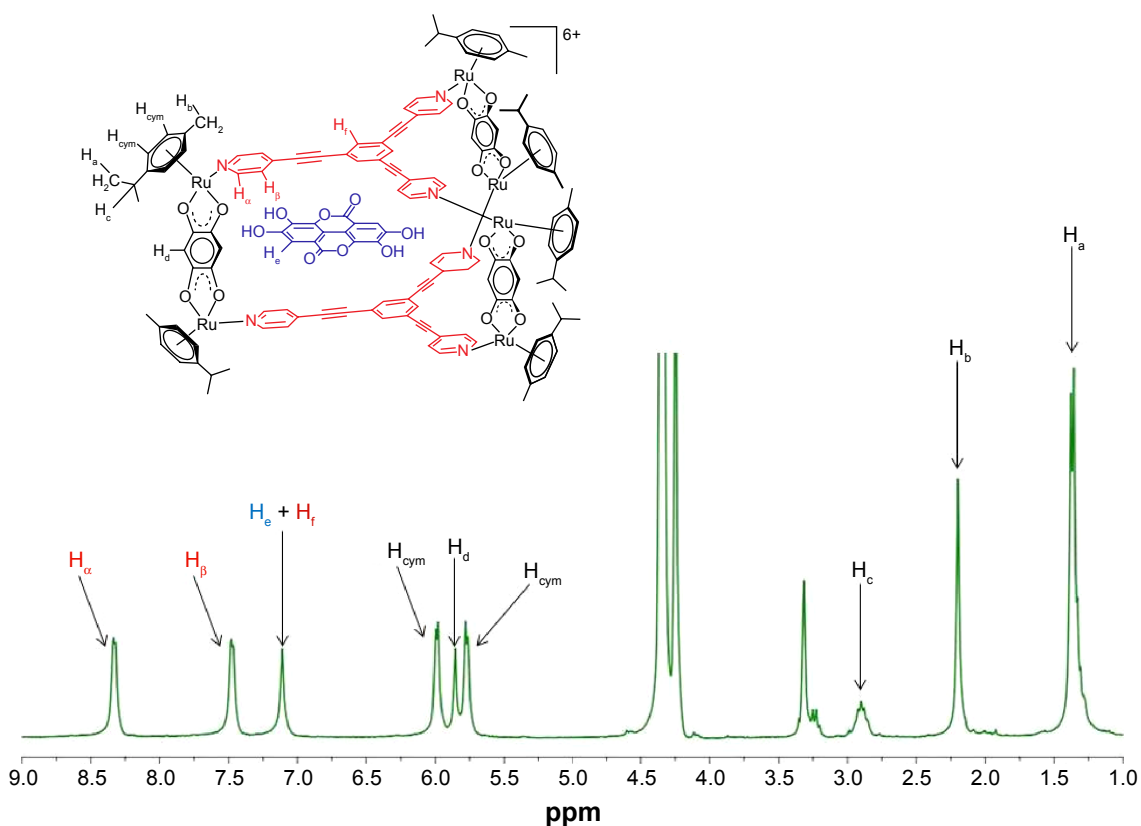


Figure S1 ^1H spectra of metalla-prismatic cage **9** recorded in $\text{CD}_3\text{NO}_2:\text{CD}_3\text{OD}$ (1:1) solution.
Abbreviation: ppm, parts per million.

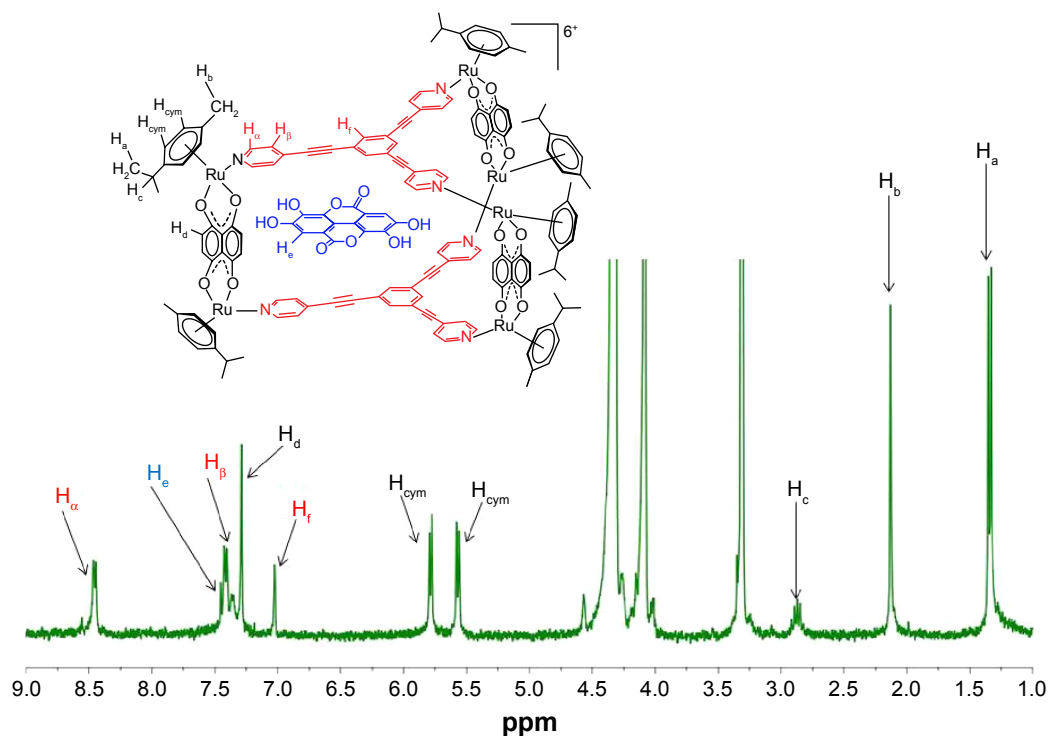


Figure S2 ^1H spectra of metalla-prismatic cage **10** recorded in $\text{CD}_3\text{NO}_2:\text{CD}_3\text{OD}$ (1:1) solution.
Abbreviation: ppm, parts per million.

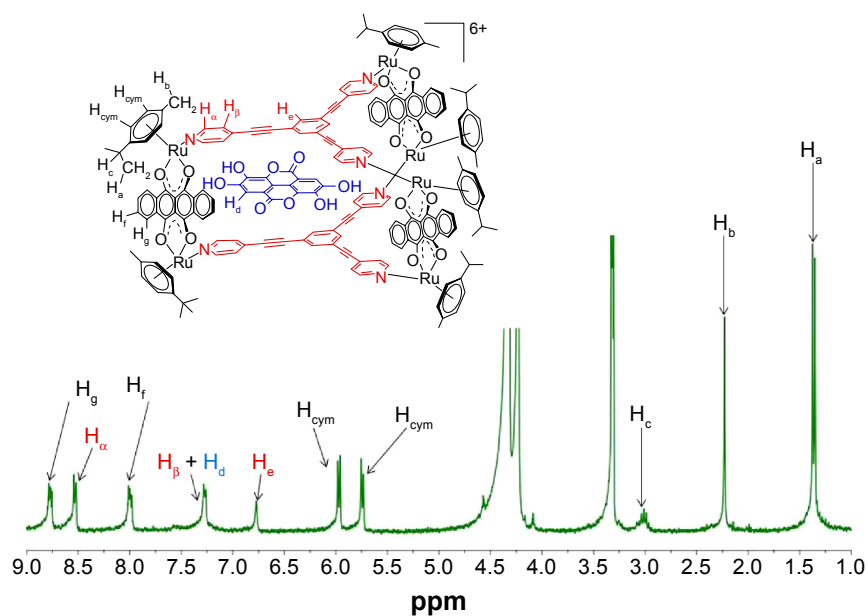


Figure S3 ^1H spectra of metalla-prismatic cage **11** recorded in $\text{CD}_3\text{NO}_2:\text{CD}_3\text{OD}$ (1:1) solution.
Abbreviation: ppm, parts per million.

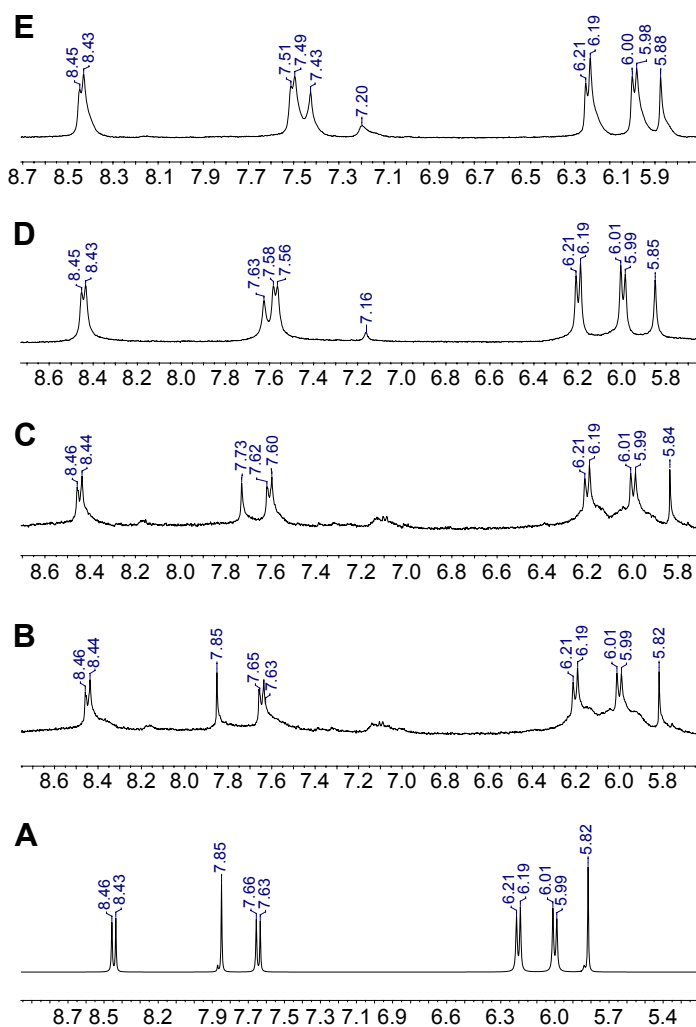


Figure S4 ^1H NMR titrations of ellagic acid in a solution of **6** in acetone- d_6 .

Notes: (A) **6** (4.0 mm), (B) **6**+0.25 equivalents of ellagic acid, (C) **6**+0.50 equivalents of ellagic acid, (D) **6**+0.75 equivalent of ellagic acid and (E) **6**+1.0 equivalents of ellagic acid.

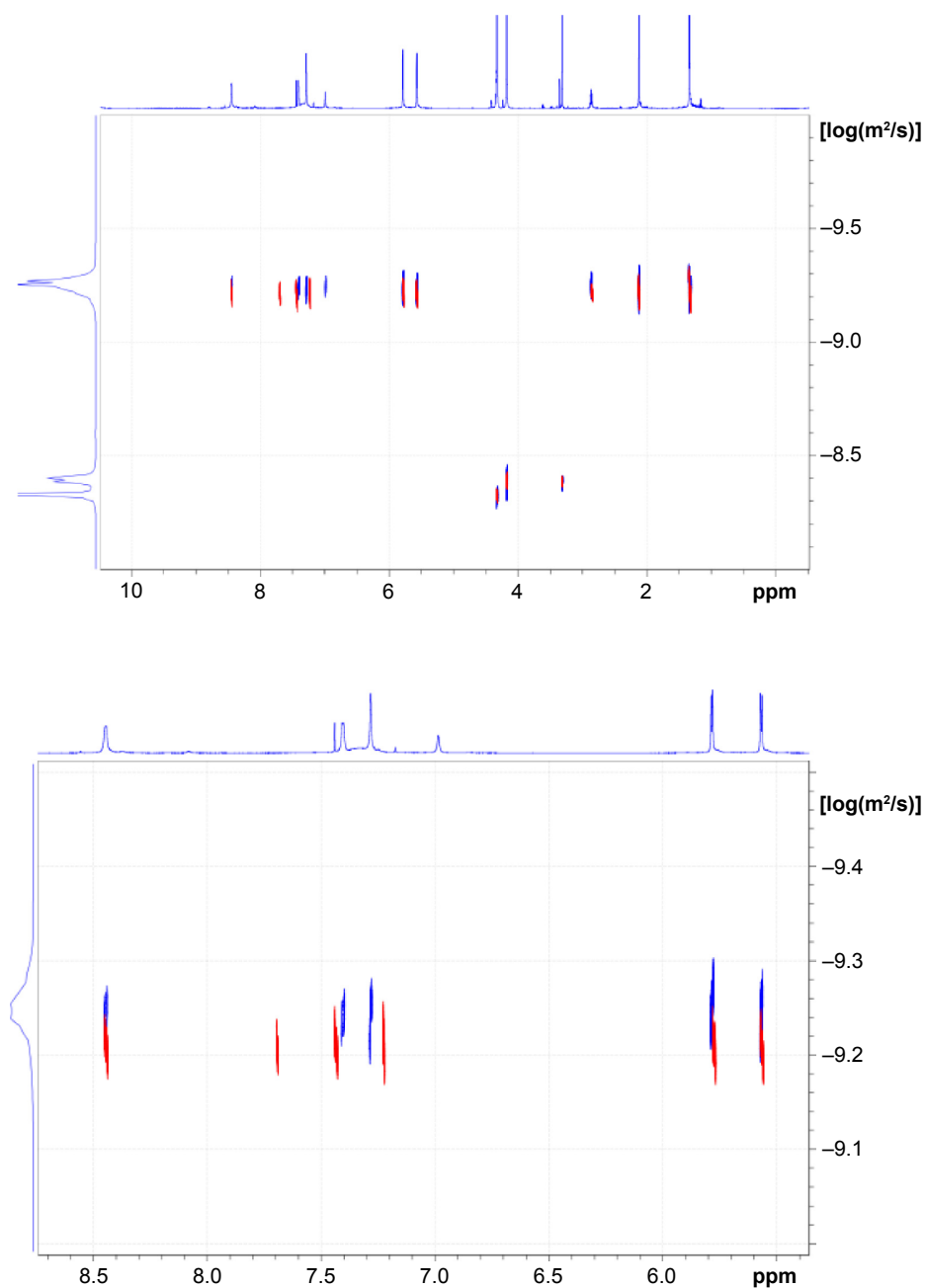


Figure S5 The DOSY spectra of **7** (red) and **10** (blue) in $\text{CD}_3\text{NO}_2\text{:CD}_3\text{OD}$ (1:1).
Abbreviations: DOSY, Diffusion-ordered NMR spectroscopy; ppm, parts per million.

International Journal of Nanomedicine

Dovepress

Publish your work in this journal

The International Journal of Nanomedicine is an international, peer-reviewed journal focusing on the application of nanotechnology in diagnostics, therapeutics, and drug delivery systems throughout the biomedical field. This journal is indexed on PubMed Central, MedLine, CAS, SciSearch®, Current Contents®/Clinical Medicine,

Journal Citation Reports/Science Edition, EMBase, Scopus and the Elsevier Bibliographic databases. The manuscript management system is completely online and includes a very quick and fair peer-review system, which is all easy to use. Visit <http://www.dovepress.com/testimonials.php> to read real quotes from published authors.

Submit your manuscript here: <http://www.dovepress.com/international-journal-of-nanomedicine-journal>